Dual phase-shift Bragg grating silicon photonic modulator operating up to 60 Gb/s

Kevin Bédard, Alexandre D. Simard, Benoit Filion, Y. Painchaud, Leslie A. Rusch, and Sophie LaRochelle

Optics Express, (Volume 24, Issue 3) (2016)

Doi: 10.1364/OE.24.002413

https://www.osapublishing.org/oe/abstract.cfm?uri=oe-24-3-2413

Dual Phase-Shift Bragg Grating Silicon Photonic Modulator operating up to 60 Gb/s

K. Bédard[1], A. D. Simard[1], B. Filion[1], Y. Painchaud[2], L. A. Rusch[1], and S. LaRochelle[1,*]

[1]*Centre d'optique, photonique et laser (COPL), Department of Electrical and Computer Engineering, Université Laval, Québec, QC, G1V 0A6, Canada*
[2] *TeraXion Inc, Québec, QC, G1P 4S8, Canada*
[*]*sophie.larochelle@gel.ulaval.ca*

Abstract: We demonstrate PAM-4 and OOK operation of a novel silicon photonic modulator. The modulator design is based on two phase-shifts in a Bragg Grating structure driven in a push pull configuration. Back-to-back PAM-4 modulation is demonstrated below the FEC threshold at up to 60 Gb/s. OOK modulation is also shown up to 55 Gb/s with MMSE equalization and up to 50 Gb/s without equalization. Eye diagrams and BER curves at different bit rates are provided for both PAM-4 and OOK modulations. To our knowledge, this structure is the fastest silicon photonic modulator based on Bragg gratings, reaching modulation speed comparable to the fastest Mach-Zehnder modulators and micro-ring modulators.

OCIS codes: (050.2770) Gratings, (130.3120) Integrated optics devices, (250.7360) Waveguide modulators

References and links

1. R. Rodes, M. Mueller, B. Li, J. Estaran, J. B. Jensen, T. Gruendl, M. Ortsiefer, C. Neumeyr, J. Rosskopf, K. J. Larsen, M. Amann, and I. T. Monroy, "High-Speed 1550 nm VCSEL Data Transmission Link Employing 25 GBd 4-PAM Modulation and Hard Decision Forward Error Correction," J. Lightwave Technol. **31**(4), 689–695 (2013).
2. K. P. Zhong, W. Chen, Q. Sui, J. Man, A. P. T. Lau, C. Lu, and L. Zeng, "Low Cost 400GE Transceiver for 2km Optical Interconnect using PAM4 and Direct Detection," in Asia Commun. Photonics Conf. 2014(Optical Society of America, 2014), paper ATh4D2.
3. S. Lange, R. Kaiser, M. Gruner, M. Hamacher, K.-O. Velthaus, and M. Schell, "Low Switching Voltage InP-Based Travelling Wave Electrode Mach-Zehnder Modulator Monolithically Integrated with DFB-Laser for 60 Gb/s NRZ," in Opt. Fiber Commun. Conf. (Optical Society of America, 2015), paper Th4E1.
4. C. Cole, "Beyond 100G client optics," IEEE Commun. Mag. **50**(2), s58–s66 (2012).
5. Y. A. Vlasov, "Silicon CMOS-integrated nano-photonics for computer and data communications beyond 100G," IEEE Commun. Mag. **50**(2), s67–s72 (2012).
6. D. Patel, S. Ghosh, M. Chagnon, A. Samani, V. Veerasubramanian, M. Osman, and D. V. Plant, "Design, analysis, and transmission system performance of a 41 GHz silicon photonic modulator," Opt. Express **23**(11), 14263 (2015).
7. M. Streshinsky, R. Ding, Y. Liu, A. Novack, Y. Yang, Y. Ma, X. Tu, E. K. S. Chee, A. E.-J. Lim, P. G.-Q. Lo, T. Baehr-Jones, and M. Hochberg, "Low power 50 Gb/s silicon traveling wave Mach-Zehnder modulator near 1300 nm," Opt. Express **21**(25), 30350 (2013).
8. R. Dubé-Demers, S. LaRochelle, and W. Shi, "Pulse Amplitude Modulation with a Femtojoule Silicon Microring Modulator at 80-Gb/s," presented at the 12th IEEE Int. Conf. Group IV Photonics, Vancouver, Canada, 26-28 Aug. 2015.
9. X. Xiao, H. Xu, X. Li, Z. Li, T. Chu, J. Yu, and Y. Yu, "60 Gbit/s Silicon Modulators with Enhanced Electro-optical Efficiency," in Opt. Fiber Commun. Conf. Fiber Opt. Eng. Conf. 2013 (Optical Society of America, 2013), paper OW4J3.
10. G. T. Reed, G. Mashanovich, F. Y. Gardes, and D. J. Thomson, "Silicon optical modulators," Nature Photonics **4**(8), 518–526 (2010).
11. A. Samani, M. Chagnon, D. Patel, V. Veerasubramanian, S. Ghosh, M. Osman, Q. Zhong, and D. V. Plant, "A Low-Voltage 35-GHz Silicon Photonic Modulator-Enabled 112-Gb/s Transmission System," IEEE Photonics J. **7**(3), 1–13 (2015).

12. M. Chagnon, M. Osman, M. Poulin, C. Latrasse, J.-F. Gagné, Y. Painchaud, C. Paquet, S. Lessard, and D. Plant, "Experimental study of 112 Gb/s short reach transmission employing PAM formats and SiP intensity modulator at 13 μm," Opt. Express **22**(17), 21018 (2014).
13. M. Poulin, C. Latrasse, J.-F. Gagne, Y. Painchaud, M. Cyr, C. Paquet, M. Morsy-Osman, M. Chagnon, S. Lessard, and D. V. Plant, "107 Gb/s PAM-4 transmission over 10 km using a SiP series push-pull modulator at 1310 nm," in Eur. Conf. Opt. Commun. (ECOC, 2014), 1–3.
14. D. Patel, A. Samani, V. Veerasubramanian, S. Ghosh, and D. V. Plant, "Silicon Photonic Segmented Modulator-Based Electro-Optic DAC for 100 Gb/s PAM-4 Generation," IEEE Photonics Technol. Lett. **27**(23), 2433–2436 (2015).
15. C. Cole, I. Lyubomirsky, A. Ghiasi, and V. Telang, "Higher-order modulation for client optics," IEEE Commun. Mag. **51**(3), 50–57 (2013).
16. D. Patel, V. Veerasubramanian, S. Ghosh, A. Samani, Q. Zhong, and D. V. Plant, "High-speed compact silicon photonic Michelson interferometric modulator," Opt. Express **22**(22), 26788–26802 (2014).
17. X. Li, X. Xiao, H. Xu, Z. Li, T. Chu, J. Yu, and Y. Yu, "Highly Efficient Silicon Michelson Interferometer Modulators," IEEE Photonics Technol. Lett. **25**(5), 407–409 (2013).
18. X. Wang, M. Caverley, J. Flueckiger, Y. Wang, N. A. F. Jaeger, and L. Chrostowski, "Silicon photonic Bragg grating modulators," in 2014 IEEE Photonics Conf. (IPC, 2014), 190–191.
19. W. Zhang, N. Ehteshami, W. Liu, and J. Yao, "Silicon-based on-chip electrically tunable sidewall Bragg grating Fabry–Perot filter," Opt. Lett. **40**(13), 3153–3156 (2015).
20. M. Caverley, X. Wang, K. Murray, N. A. F. Jaeger, and L. Chrostowski, "Silicon-on-Insulator Modulators Using a Quarter-Wave Phase-Shifted Bragg Grating," IEEE Photonics Technol. Lett. **27**(22), 2331–2334 (2015).
21. P. P. Absil, P. De Heyn, H. Chen, P. Verheyen, G. Lepage, M. Pantouvaki, J. De Coster, A. Khanna, Y. Drissi, D. Van Thourhout, and J. Van Campenhout, "Imec iSiPP25G silicon photonics: a robust CMOS-based photonics technology platform," Proc. SPIE 9367, 93670V – 93670V – 6 (2015).
22. M.-J. Picard, Y. Painchaud, C. Latrasse, C. Larouche, F. Pelletier, and M. Poulin, "Novel Spot-Size Converter for Optical Fiber to sub-um Silicon Waveguide Coupling with Low Loss, Low Wavelength Dependence and High Tolerance to Alignment," in Eur. Conf. Opt. Commun. (ECOC, 2015), paper Mo.4.2.4.
23. A. D. Simard and S. LaRochelle, "Complex apodized Bragg grating filters without circulators in silicon-on-insulator," Opt. Express **23**(13), 16662 (2015).
24. E. Ip and J. M. Kahn, "Digital Equalization of Chromatic Dispersion and Polarization Mode Dispersion," J. Lightwave Technol. **25**(8), 2033–2043 (2007).
25. A. D. Simard, N. Ayotte, Y. Painchaud, S. Bedard, and S. LaRochelle, "Impact of sidewall roughness on integrated Bragg gratings," J. Lightwave Technol. **29**(24), 3693–3704 (2011).
26. A. D. Simard, G. Beaudin, V. Aimez, Y. Painchaud, and S. LaRochelle, "Characterization and reduction of spectral distortions in silicon-on-insulator integrated Bragg gratings," Opt. Express **21**(20), 23145–23159 (2013).
27. H. Xu, X. Xiao, X. Li, Y. Hu, Z. Li, T. Chu, Y. Yu, and J. Yu, "High speed silicon Mach-Zehnder modulator based on interleaved PN junctions," Opt. Express **20**, 15093 (2012).
28. B. D. Xiaotie Wu, "A 20Gb/s NRZ/PAM-4 1V transmitter in 40nm CMOS driving a Si-photonic modulator in 0.13μm CMOS," Dig. Tech. Pap. - IEEE Int. Solid-State Circuits Conf. (ISSCC, 2013), 128–129.
29. S. S. Azadeh, F. Merget, S. Romero-García, A. Moscoso-Mártir, N. von den Driesch, J. Müller, S. Mantl, D. Buca, and J. Witzens, "Low Vπ Silicon photonics modulators with highly linear epitaxially grown phase shifters," Opt. Express **23**(18), 23526–23550 (2015)

1. Introduction

Data center bandwidth requirements increase with the growing popularity of video streaming and cloud computing, pushing development of 100G and 400G short data links (500m to 2km) over single-mode fibers. In the absence of a clear consensus on how to reach the size and cost targets for these links, several technologies are currently being considered: directly modulated lasers (DML), such as long-wave vertical-cavity surface-emitting lasers (VCSELs) [1], electroabsorption modulated laser (EML) [2], indium phosphide modulators [3] and silicon modulators [4]. Silicon photonics (SiP) is a technology with great potential for data centers due to its high level of device integration, low-power operation and cost effectiveness [5].

Research on high performance SiP optical modulators has focused on Mach-Zehnder (MZM) and micro-ring modulators (MRM). Both types of modulator have achieved high bandwidth and low power consumption [6–9], with good extinction ratio and manageable insertion losses [10]. The main advantages of MZMs are typically its wide optical bandwidth,

low chirp and small temperature sensitivity, while MRMs are characterized by small footprint and low power consumption. The use of higher modulation formats is an additional means to increase the capacity of high speed short data links and, recently, high speed pulse amplitude modulation (PAM) has been demonstrated using MZMs [11–13], segmented electrode MZMs [14] and MRMs [8]. PAM is of particular interest due to its high spectral efficiency and compatibility with direct detection [15].

In addition to MZMs and MRMs, other integrated SiP modulator structures, such as Michelson interferometric modulators (MIM) [16,17], have been successfully developed to achieve efficient modulation, using a lumped-element electrode, by exploiting the fact that the light travels twice through the PN junction phase-shifter. However, until now, little effort has been devoted to develop integrated Bragg grating (IBG) modulators. The complex dependency between the grating parameters (coupling coefficient, grating length, apodisation profile, etc.) and the modulator figure-of-merits (insertion loss, modulation bandwidth, extinction ratio, driving voltage, etc.) led to modulators that, until now, are characterized by high insertion loss [18] (> 10 dB excluding the coupling loss) and low modulation bandwidth (~7-10 GHz [18,19] and 3.5 Gb/s NRZ [19]). Only very recently was transmission below the FEC threshold achieved at 25 Gb/s [20], but this performance is still far from MZM and MRM.

In this paper, we demonstrate an IBG modulator attaining 50 Gb/s with on-off keying (OOK). This achievement represents an important improvement over previous IBG modulator designs and these results place IBG modulators as important contenders for high speed solutions along with SiP MZMs [12] (70 Gb/s) and MRMs [8] (66 Gb/s). The tested IBG modulator reached 60 Gb/s when combining pulse amplitude modulation (PAM) with digital signal processing (DSP) at the receiver, i.e. post-compensation. This data rate approaches the 80 Gb/s recently reported for a MRM [8] using PAM and similar DSP. Faster data rates (112 Gb/s with PAM-4 and PAM-8) have been reported for a SiP MZM [12,13]; however these demonstrations involved the use of both pre- and post-compensation. For pre-compensation, additional hardware is required (a digital-to-analog converter) that increases cost, size and power consumption.

In this paper, we describe and experimentally demonstrate a high speed IBG modulator. We also discuss further improvements to the design that would enhance their performance. In section 2, the operating principle of the modulator is first presented while section 3 shows the static spectral responses. Section 4 presents the transmission testbed and BER measurement results for OOK and PAM-4, with and without post-equalization. A short discussion follows in section 5 on the tradeoffs inherent to this kind of modulator.

2. Design

Fig. 1(a) shows the schematic of the SiP dual phase-shift Bragg grating modulator. The IBG has a uniform period profile with two π-phase shifts located at $L/4$ and $3L/4$, where L is the grating length. The two phase shifts define two in-phase resonant cavities that provide a transmission peak at the center of its reflection band as shown by the blue line in Fig. 1(b). Two PN junctions are added on each side of the structure to modulate the effective index independently for each half of the grating structure. We operate the modulator in a push-pull manner around the bias point, i.e. shifting the resonance of one cavity towards shorter wavelength and the other towards higher wavelengths in the presence of a mark (binary "1"). When the cavities are no longer in phase, the transmission peak splits in two resulting in a reduced amplitude at the central wavelength as shown in the red solid line in Fig. 1(b). The dual phase shift design provides a wider transmission peak than its single phase-shift counterpart of the same length L and equal coupling coefficient (black dotted line in Fig. 1(b)) which improves the modulator stability. Furthermore, the dual phase-shift configuration operates the modulator at the central wavelength of the peak, thus reducing the chirp of the output signal, which can also improve the transmission performance at very high bit rate.

The inset of Fig. 1(a) shows that the lateral PN junctions use three doping levels with positions that were chosen to minimize optical losses while keeping the resistance as low as

possible to insure high speed operation. The PN junctions are symmetric. The electrodes are coplanar strip waveguides (CPS) designed to have a 50 Ω impedance.

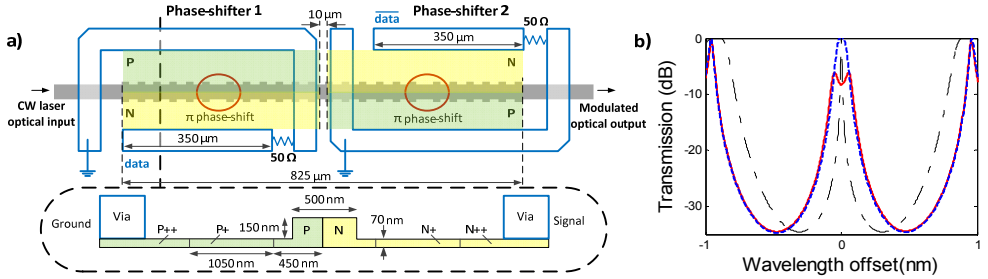

Fig. 1: a) Schematic of the dual phase-shift Bragg grating modulator. b) Typical spectra with (red, solid) and without (blue, dashed) bias voltages applied to the PN junctions; a typical spectrum for a Bragg grating with a single π phase-shift is also shown (black, dotted).

3. Fabrication and static response

The modulator structure was fabricated using the IMEC ISIPP25G [21] process, which features 193 nm optical lithography, a 220 nm top-silicon layer and a 2 µm buried oxide layer. Three etch depths are used for this design: full etch for routing waveguides, deep etch for the IBG modulator (leaving a slab of ~70 nm), and shallow etch for the focusing grating couplers used as input and output to the device [21]. The 825 µm long IBG is composed of 30 nm sidewall corrugations in a 500 nm wide waveguide. The grating has a period of 315 nm and a 50% duty cycle. The geometry of the two 350 µm long depletion-based phase-shifters, composed of three levels of p and n dopant, is shown in the inset of Fig. 1(a). They are located on each side of the IBG and are driven with 50 Ω terminated CPS. Their length was maximized to accommodate the bent CPSs at the center of the IBG. As a result, there is a gap of 125 µm between the two PN phase-shifters.

Fig. 2(a) shows the modulator static spectral response in reflection and transmission measured with a wavelength swept interferometer (OVA, Luna Technology). Fig. 2(b) shows the transmission peak for different bias voltages. One on-chip y-branch is placed before the modulator to simplify reflection measurements. The total loss of the system is 19.5 dB and can be explained as follows: 10.8 dB from the two grating couplers, typical 2.5 dB propagation loss from the 1 cm-long routing waveguide, 3.4 dB from the y-branch (3 dB splitting + 0.4 dB excess losses) and about 2.8 dB from the doped section of the Bragg modulator that cover almost all the modulator length (i.e. when no bias is applied, the propagation loss in the grating is evaluated to be 34.5 dB/cm over a length of 815 µm). The losses could be decreased significantly by using Si_3N_4 multi-rod edge couplers [22] instead of grating couplers, by implementing an IBG configuration without a y-branch [23] and by minimizing the routing waveguides length.

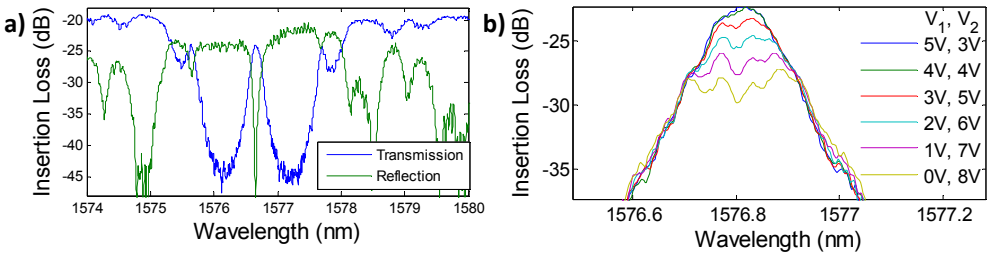

Fig. 2: (a) Transmission and reflection spectra of the IBG without DC bias, (b) close up on the transmission peak measured for different bias voltages. The legend indicates the reverse bias voltage of the first electrode (left) and the second electrode (right).

4. System tests

The modulator performance was characterized with OOK and PAM-4 modulation with the experimental setup shown in Fig. 3. Pseudo random bit sequences (PRBS) with lengths of 2^{15}-1 are first generated by a bit pattern generator (BPG) (SHF 12103A). The Bragg modulator requires two PRBS for PAM-4 generation and one PRBS for OOK generation. For PAM-4 experiments (block A in Fig. 3), a digital to analog converter (DAC) (SHF 611C) is used to drive the modulator: the DAC non-inverted (*data*) and inverted ($\overline{data}$) outputs are used to drive the modulator in a push-pull configuration. External tuneable delay lines (TDLs) are used to synchronise the two RF signals. For OOK experiments (block B in Fig. 3), *data* and $\overline{data}$ are taken directly from the BPG outputs and the synchronisation is done with the skew control of the BPG. Next, the RF signals are amplified and bias-tees are used to combine them with the DC reverse bias voltage of each PN junction. For all experiments, the modulation peak-to-peak voltage is set to 4.5 V, while the reverse bias voltages are set to V_1 = 1.8 V and V_2 = 6.4 V. The 4.6 V difference in the bias voltage was necessary to align the two resonances at the same wavelength thus compensating fabrication imperfections. The optical wavelength is set around 1577.05 nm throughout the experiments (the laser wavelength is slightly adjusted to compensate temperature shifts). The laser output power is set to 13 dBm and a polarization controller (PC) is placed before the modulator to maximize the fiber-to-chip coupling in the fundamental TE mode.

To compensate the optical loss of the device, we inserted a semiconductor optical amplifier (SOA). The SOA is followed by a tunable optical bandpass filter set at a 3-dB bandwidth of 0.8 nm and an inline attenuator is used to sweep the received power. The eye diagrams were captured using the optical port of an 80 GHz bandwidth sampling oscilloscope (SO) (block D in Fig. 3). For BER measurements up to 30 Gb/s the optical signal is converted into an electrical signal via a 70 GHz U2T photodetector (PD) and then sampled by a real time oscilloscope (RTO) at 80 GSa/s with a 30 GHz electrical bandwidth (block C in Fig. 3). For measurements over 30 Gb/s, a RTO at 200 GSa/s with a 70 GHz electrical bandwidth was used. For all the measurements, four million samples were captured in order to yield reliable BER values.

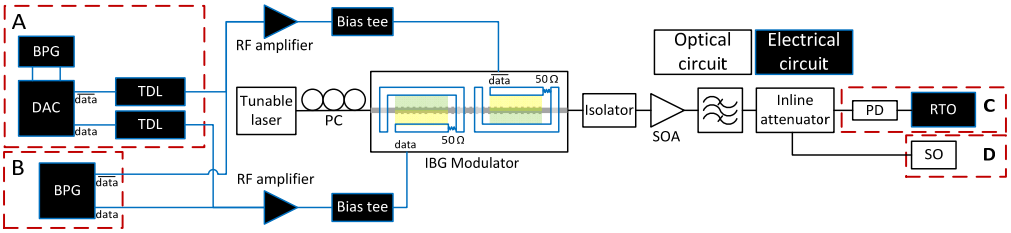

Fig. 3: Experimental setup used to measure the BER (block C) and the eye diagrams (block D) with PAM-4 (block A) and OOK (block B) modulation.

Following data acquisition, a second order Gaussian low-pass filter with a 3-dB bandwidth set to twice the bit rate is applied and resampling at 2 samples/symbol is performed. The BER is calculated with and without post-compensation. With post-compensation, a minimum mean square error (MMSE) equalizer is applied [24]. The number of taps of the MMSE equalizer should be low enough to ensure low processing complexity and power consumption since the training sequences induce latency and power overheads. We found that 50 taps trained over 2000 symbols were the smallest values that could be used without sacrificing performance. Once the MMSE tap weights are fixed, the decision threshold and sampling time are optimized to minimize the BER and the BER are calculated for all the captured symbols.

Fig. 4 shows sampled eye diagrams (with identical vertical scale) with a received averaged power of 1 dBm: open eye diagrams are obtained for all bit rates. Note that for PAM-4, the

full signal amplitude at 50 Gb/s and 60 Gb/s is slightly lower compared to 25 Gb/s. Fig. 5 shows the BER without (solid lines) and with post-compensation (dashed lines) as a function of received power. Assuming a FEC threshold of 3.8×10^{-3} [12 and references therein], error-free OOK transmission was obtained for rates up to 55 Gb/s and 50 Gb/s with and without post-compensation respectively. Post-compensation allowed for 1-2 dB increase in power margin at bit rates of 30 Gb/s and beyond. Overall, post-compensation marginally improves the performance. For PAM-4 experiments, BER below the FEC threshold is obtained up to 60 Gb/s with post-compensation. While the eye for 55 Gb/s OOK is more open than 60 Gb/s PAM-4, PAM-4 achieved higher bit rate at lower received power. At 50 Gb/s, PAM-4 reached the FEC threshold at lower received power.

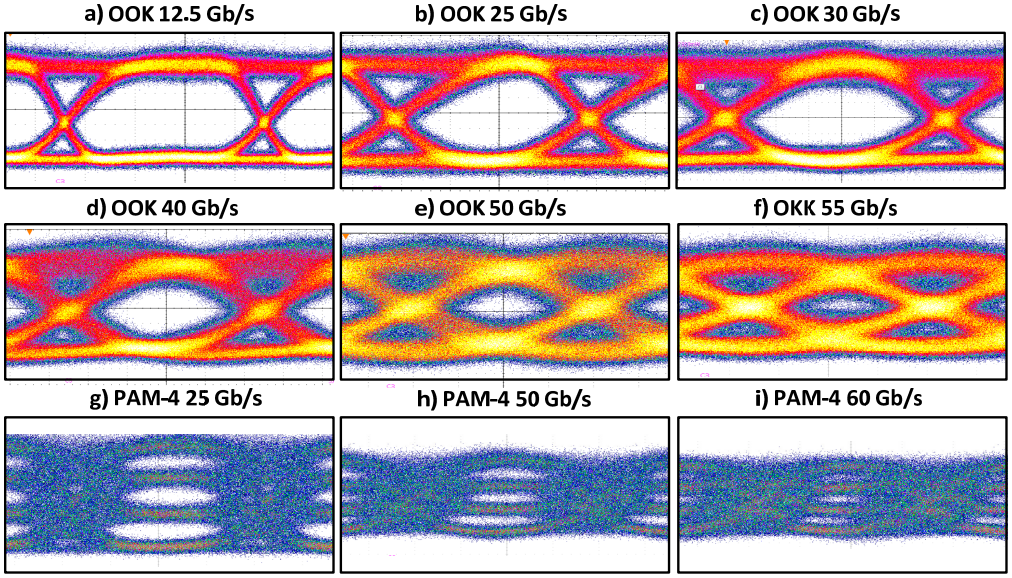

Fig. 4: Eye diagrams for different bit rates and modulation format with a received power of 1 dBm. The optical power is displayed on a linear scale with the height of the black boxes corresponding to an optical power difference of 3 mW.

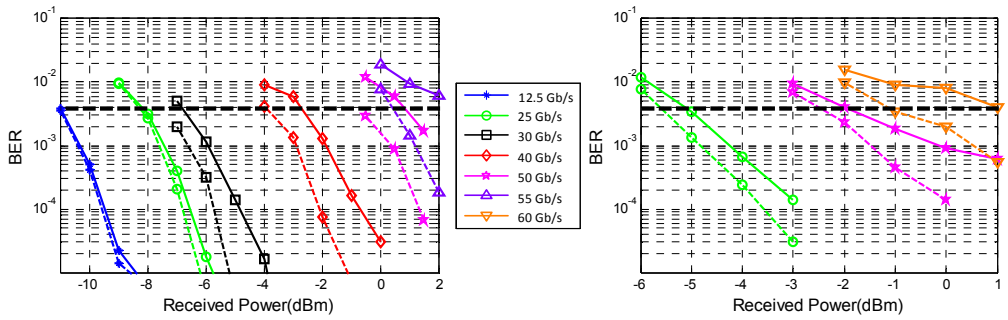

Fig. 5: BER vs. received power for different bit rates: (a) OOK, (b) PAM-4. Dotted lines with equalization, solid lines without.

5. Discussion

In this paper, we demonstrate that dual phase-shift Bragg grating modulators are a novel modulator structure that can provide large modulation bandwidth, in the present case allowing transmission exceeding 50 Gbit/s. Nonetheless, many aspects of Bragg modulators remain to

be explored in order to fully optimize not only its operating bandwidth, but also its power consumption.

For higher bit rate operation, optimisation of the grating profile with a dynamic model will be necessary to explore trade-offs between the grating coupling coefficient, the grating length, and the fabrication tolerance of the process. These need to be studied with the goal of reaching a CMOS compatible driving scheme. Particularly, the use of gratings operated in reflection could provide faster responses. Whether a transmissive or reflective approach is used, losses should be minimized, which implies avoiding y-branches in the latter case. For these reflective modulators, an alternative is to use interferometric structures as described in [23].

Due to its short length and resonant nature of the modulator, the power consumption of IBG modulators is expected to be between values observed in MZMs and MRMs approaches. In a modulator using traveling-wave electrodes terminated with a 50 Ω resistance, the power is mainly dissipated at the termination [16]. Power consumption in such modulators can be estimated by considering both the dynamic power consumption from the modulating driving voltage and the static power consumption contribution from the bias voltage. Regarding the dual phase-shift Bragg grating modulator, the calculated OOK power consumption at 50 Gb/s is 21.7 pJ/bit. Its power consumption could be lowered by using shorter electrodes without termination and driven by an impedance-matched CMOS driver. Without terminations, the power consumption would come mainly from the PN junction capacitance [16] leading to power consumption similar to the one reported in [20]. The bias voltage could also be lowered by reducing the mismatch between the two resonant cavities through the use of Bragg grating phase noise reduction techniques [25,26]. More efficient phase-shifters based on an interleaved PN junction [27], a SISCAP junction [28] or vertical junctions [29] could also help achieving lower driving voltages and lower bias voltages. Finally, similarly to high-Q MRM, the required driving voltage could be lowered by increasing the grating strength, which illustrates the need for future work in the codesign of the electrical and optical aspects of this modulator to achieve optimal power consumption.

6. Conclusion

A dual-phase shift Bragg grating silicon photonic modulator achieved up to 55 Gb/s transmission using OOK and up to 60 Gb/s using PAM-4 with equalization. Without equalization nor pre-compensation, BER below the FEC threshold was achieved up to 50 Gb/s for both modulation formats. All results were obtained using a SOA to overcome coupling loss, and therefore our characterizations are valid for an integrated solution using semiconductor based amplification. Further enhancement of the performance of these high speed Bragg grating modulators is expected through detailed modeling of their dynamic responses.

Acknowledgments

The SPEED research project (Silicon Photonic Electrically Engineered Devices) is funded by NSERC (RDCPJ438811-12), PROMPT (PJT-2011-17), and TeraXion. We also acknowledge the contribution and technical support of CMC Microsystems. This work is part of the Canada Research Chair program in Advanced photonic technologies for communications (APTEC).